

AD-785 688

**BOUNDARY-LAYER STUDIES ON SPINNING  
BODIES OF REVOLUTION**

**Walter B. Sturek**

**Ballistic Research Laboratories  
Aberdeen Proving Ground, Maryland**

**1973**

**DISTRIBUTED BY:**

**NTIS**

**National Technical Information Service  
U. S. DEPARTMENT OF COMMERCE  
5285 Port Royal Road, Springfield Va. 22151**

AD 785688

BOUNDARY-LAYER STUDIES ON SPINNING  
BODIES OF REVOLUTIONWALTER B. STUREK, Ph.D.  
U.S. Army Ballistic Research Laboratories  
Aberdeen Proving Ground, Maryland

## 1. INTRODUCTION

The Magnus force, as shown in Figure 1, is a side force that occurs on a spinning projectile in flight at angle of attack. This force and its associated moment are usually small (typically 1/100 to 1/10 of the normal force). However, the effect of Magnus on a projectile's aerodynamic behavior is important because it exerts an undamping force over the entire flight of the projectile. It is well known that the Magnus force can cause a projectile to become aerodynamically unstable in flight.

Recent Army interest in increasing the effective range of conventional artillery has led to the design of projectile shapes that have long slender forebodies, short cylindrical portions, and boattailed afterbodies. These design characteristics have resulted in decreased aerodynamic drag, hence a greater range capability; however, these shapes are aerodynamically less stable than conventional shapes. The decreased aerodynamic stability of these new shapes results in a greater sensitivity to a Magnus induced instability.

Although Magnus is an important consideration in the design of artillery projectiles, no procedure exists for accurately estimating Magnus effects that is sufficiently general in application to be useful to the artillery projectile design engineer.

STUREK

The Magnus effect has been modeled theoretically<sup>(1),(2),(3)</sup> as being caused by spin induced distortion of the boundary-layer. This yields an effective projectile body shape that is asymmetric with respect to the plane of the angle of attack as shown in Figure 2. This results in an asymmetric pressure distribution about the projectile that yields a net side force. Other mechanisms that contribute to the Magnus effect are asymmetry in the pressure distribution through the boundary-layer and asymmetry in the distribution of wall shear stress on the ogive portion of projectiles<sup>(4)</sup>. When boundary-layer transition occurs on a projectile, spin acts to distort the location of boundary-layer transition as well as the subsequent turbulent boundary-layer development. Jacobson<sup>(3),(4)</sup> has suggested that this case would be of critical importance in affecting the aerodynamic behavior of projectiles.

This paper describes some results from a series of experimental studies of the viscous boundary-layer on spinning bodies of revolution. The objectives of these studies are: (1) provide data which will help guide the development of a useful procedure for computing Magnus effects on aerodynamic shapes of interest in artillery projectile design; (2) verify the significance of the boundary-layer configuration--laminar, transitional, turbulent--on the resulting Magnus force; and (3) develop a better understanding of the physics of the three-dimensional boundary-layer on spinning bodies of revolution at angle of attack.

## 2. EXPERIMENTAL PROCEDURE

Tests have been conducted using two models--a 10° half angle cone<sup>(5)</sup> with a base diameter of 7.78 cm and a six caliber tangent-ogive-cylinder model with a one caliber ogive and 5.08 cm base diameter. The experiment consisted of two phases: (1) an optical study of the boundary-layer on the spinning models using spark shadowgraphs and; (2) direct measurement of the normal and side forces on the spinning models using the strain gage balance technique.

### 2.1 Optical Study

The boundary-layer on a model viewed in a wind tunnel is visible at two positions--the upper and the lower surface. By mounting the model on an offset strut and then rotating the model

## STUREK

in increments about the axis of the strut, the boundary-layer can be viewed over the entire surface of the model. This technique has been used to obtain spark shadowgraphs showing the boundary-layer development completely about the circumference of the two models. Spark shadowgraphs were taken of these models for spin rates up to 30,000 RPM, for  $\alpha = 2^\circ$  and  $4^\circ$ , and  $M = 2, 3,$  and  $4$ . For these tests, the tunnel total pressure was adjusted to a high value so that the boundary-layer underwent natural transition from laminar to turbulent completely about the circumference of the model before reaching the base. Examples of the spark shadowgraphs are shown in Figures 3 and 4. Figure 5 shows the coordinate system and the sign convention used for azimuthal angle.

### 2.2 Strain-Gage Balance Measurements

The Magnus and normal forces on the models were measured using the strain-gage balance technique. The Magnus force measurements were made while holding the model at a fixed angle of attack with data being recorded on magnetic tape as the models coasted down from a spin rate of 35,000 RPM. The spin down time for the cone model was three minutes and that for the tangent-ogive-cylinder model was six minutes. Normal force measurements were recorded with the Magnus force measurements and also while pitching the models slowly through an angle of attack range from  $+10^\circ$  to  $-6^\circ$ .

Magnus force measurements were obtained for three significantly different boundary-layer configurations: (1) low tunnel  $p_o$  -- predominately laminar boundary-layer; (2) high tunnel  $p_o$  -- natural transition to turbulent completely about the model; and (3) high tunnel  $p_o$  -- boundary-layer tripped to turbulent using a band of #80 grit placed one inch from the model leading edge. These measurements were made for  $M = 2, 3,$  and  $4$ .

## 3. EXPERIMENTAL RESULTS

### 3.1 Optical Study

The location of boundary-layer transition was determined from the spark shadowgraphs as that position where a ropiness or turbulent structure was completely established in the boundary-layer. No effort has been made to relate this criteria for the location of boundary-layer transition to conventional criteria such as wall heat transfer, wall shear stress, or wall pressure fluctuation intensity.

STUREK

Examples of the data showing the profile of the location of boundary-layer transition for both models are shown in Figures 6 and 7. For the cone model, the distance from the center of the circle to the data point represents the distance from the tip of the cone, along a ray of the cone, to the location of boundary-layer transition. For the tangent-ogive-cylinder model, each data point represents the distance from the base of the model along a ray of the cylinder to the location of boundary-layer transition. The data clearly show that surface spin distorts the profile of boundary-layer transition with respect to the plane of angle of attack from symmetric for zero spin to increasingly asymmetric for increasing spin rates. The trends indicated by these data are: (1) transition is delayed where the cross flow velocity adds to the spin velocity; and (2) transition occurs earlier where the cross flow velocity opposes the spin velocity.

The apparent thickness of the boundary-layer at the base of the cone model was also determined from the spark shadowgraphs. A sample of these data showing the spin induced distortion of the profile of boundary-layer thickness is given in Figure 8. The profile for zero spin is symmetric with respect to the plane of angle of attack ( $\phi = 180^\circ$ ); but the profile becomes increasingly asymmetric as the spin velocity is increased.

### 3.2 Strain-Gage Balance Measurements

Representative examples of the Magnus force measurements are shown in Figures 9 and 10. The data are plotted as Magnus force coefficient versus nondimensional spin rate comparing results for different boundary-layer configurations. For the cone model, there is a substantial change in the magnitude of the Magnus force for the different boundary-layer configurations; however, the Magnus force for the tangent-ogive-cylinder model is only moderately influenced. Of particular interest, see Figure 9, is the decreased magnitude and increased linearity with spin rate of the Magnus force for the tripped turbulent boundary-layer compared to that for the predominately laminar boundary-layer. Increased linearity of the Magnus force with spin rate is also indicated in Figure 10 for the tripped turbulent boundary-layer data. In comparing the results for the two models, it is apparent that the Magnus force on a projectile shape with a long, slender ogive section could be strongly influenced by the location of boundary-layer transition. These data also suggest that the influence of boundary-layer transition on the Magnus characteristics of low-drag projectiles could be reduced by tripping the boundary-layer.

STUREK

#### 4. CONCLUDING REMARKS

The objective in obtaining the experimental data described here has been to establish the behavior of the boundary-layer on a spinning body in supersonic flow both quantitatively and qualitatively so that a valid theoretical procedure can be developed for calculating Magnus effects which will be useful in the design of artillery projectiles. Magnus data previously accumulated without knowledge of the boundary-layer configuration on the test model are of questionable value in attempting to evaluate a theoretical analysis of the Magnus effect. The data shown here represent the first detailed effort to correlate the boundary layer development over the entire surface of a spinning model in supersonic flow with direct measurements of the Magnus force. The trends indicated in sections 3.1 and 3.2 are trends that a proposed calculation scheme must be capable of predicting before that scheme can be considered a valid theoretical approach. The data shown here are only representative samples-- complete, detailed tabulations of the experimental data have been published in reference 5 for the cone model; and the data for the tangent-ogive-cylinder model will be published as a BRL report in the near future.

#### REFERENCES

1. J. C. Martin, "On Magnus Effects Caused by Boundary Layer Displacement Thickness on Bodies of Revolution at Small Angles of Attack," BRL Report No. 870 (Revised), U.S. Army Ballistic Research Laboratories, Aberdeen Proving Ground, Maryland, June 1955. AD 72055.
2. Ira D. Jacobson, "Influence of Boundary Layer Transition on the Magnus Effect on a Spinning Body of Revolution," PhD Dissertation, University of Virginia, June 1970.
3. R. Sedney, "Laminar Boundary Layer on a Spinning Cone at Small Angles of Attack in Supersonic Flow," Journal of the Aeronautical Sciences, Vol. 24, No. 6, June 1957, pp. 430-436.
4. Ira D. Jacobson, "Contribution of a Wall Shear Stress to the Magnus Effect on Nose Shapes," to be published as a BRL Contractor Report.
5. Walter B. Sturek, "Boundary Layer Studies on a Spinning Cone," BRL Report No. 1649, U.S. Army Ballistic Research Laboratories, Aberdeen Proving Ground, Maryland, May 1973. AD 762564.

## STUREK

### NOMENCLATURE

$C_N$	normal force coefficient, $F_N/qS$
$C_Y$	Magnus (side) force coefficient, $F_Y/qS$
$D$	diameter of model base, $D = 7.78$ cm for cone $D = 5.08$ cm for tangent-ogive-cylinder model
$F_N$	normal force
$F_Y$	side force
$\ell$	model length, $\ell = 22.05$ cm for cone $\ell = 30.48$ cm for tangent-ogive-cylinder model
$M$	Mach number
$p_0$	tunnel total pressure, measured in the supply header
$P$	spin rate, radians per second
$q$	dynamic pressure, $\rho V^2/2$
$Re_D$	Reynolds number, $\rho VD/\mu$
$Re_\ell$	Reynolds number, $\rho V\ell/\mu$
$S$	reference area, base of model, $\pi D^2/4$
$V$	free stream velocity
$\alpha$	angle of attack
$\mu$	molecular viscosity of air
$\rho$	free stream density
$\phi$	azimuthal angle, see Figure 4
$\omega$	spin rate, RPM

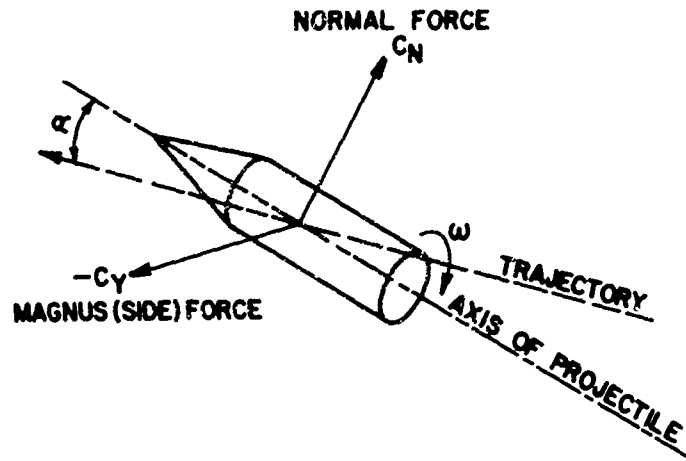


Figure 1. Magnus and Normal Forces on a Spinning Body

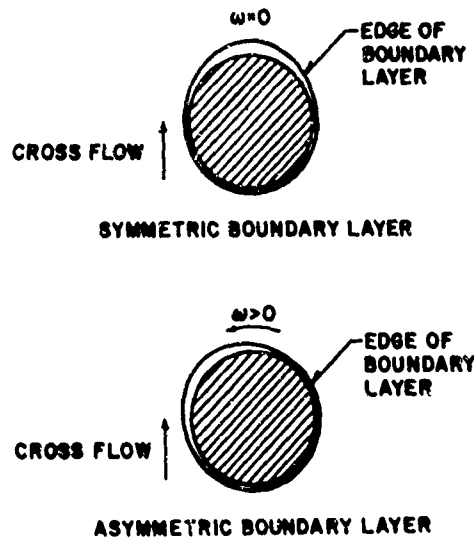


Figure 2. Cross-Sectional View of an Axisymmetric Body Illustrating Spin Induced Boundary-Layer Distortion



Figure 3. Spark Shadowgraph of Flow Over the Tangent-Ogive-Cylinder Model,  
 $M = 3$ ,  $Re_D = 1.1 \times 10^6$ ,  $\alpha = 2^\circ$ ,  $\phi = 0^\circ$ ,  $\omega = 0$

STUREK

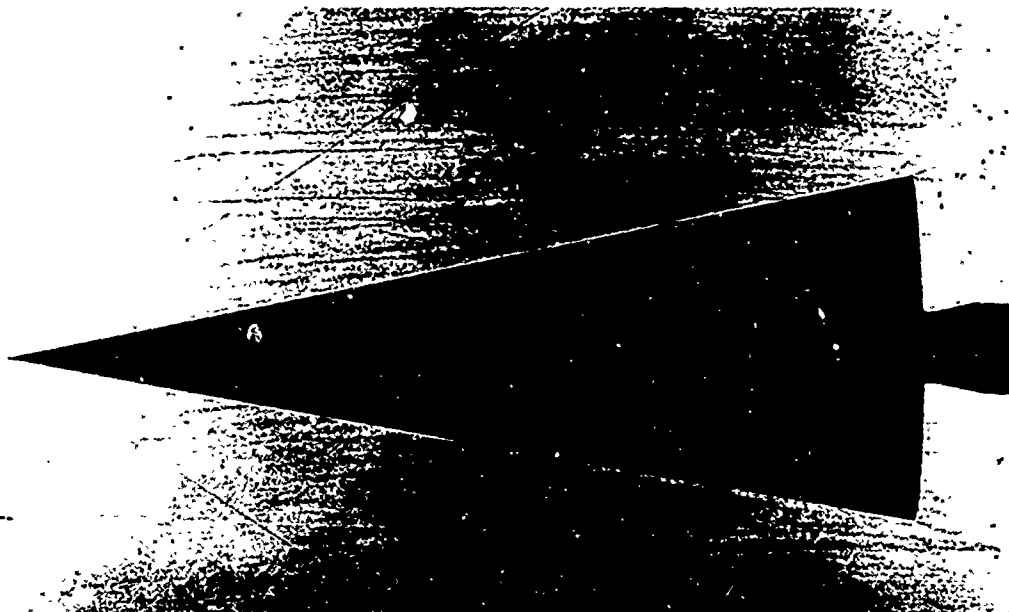


Figure 4. Spark Shadowgraph of Flow Over the Cone Model,  $M = 2$ ,  
 $Re_{\ell} = 4.75 \times 10^6$ ,  $\alpha = 2^\circ$ ,  $\phi = -60^\circ$ ,  $\omega = 18,000$  RPM

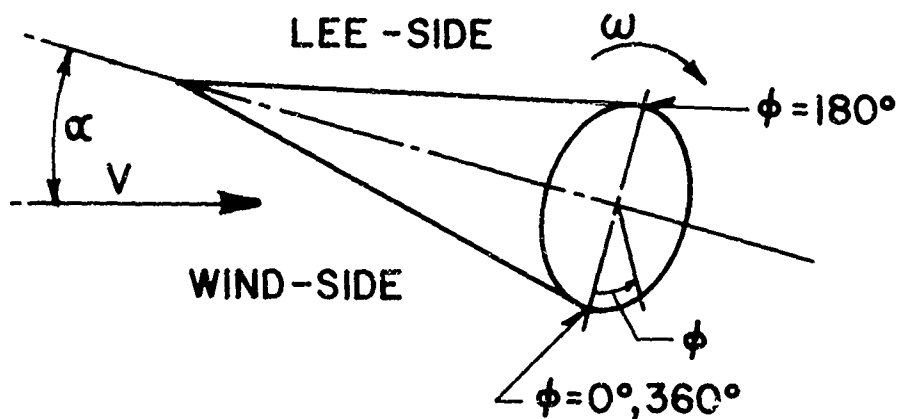


Figure 5. Coordinate System for Cone and  
Tangent-Ogive-Cylinder Models

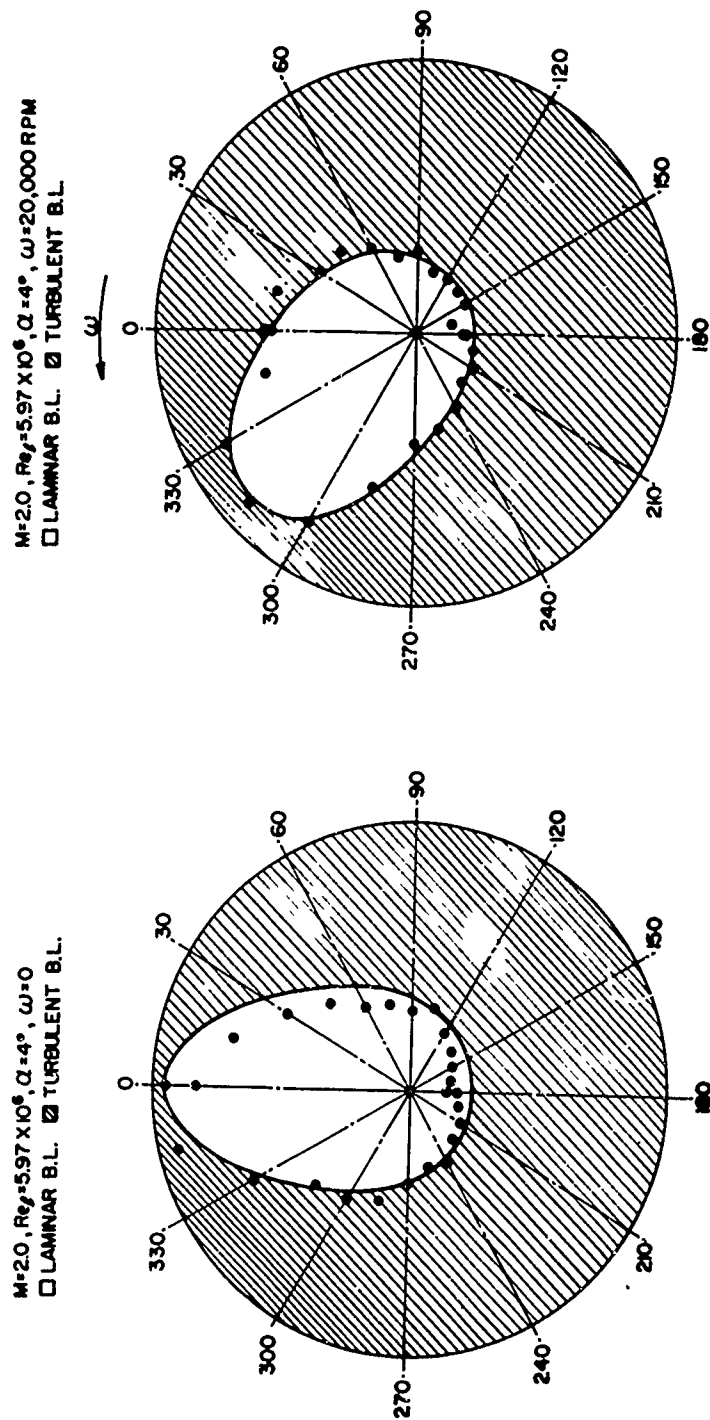


Figure 6. Profile of Boundary-Layer Transition About Circumference of  $10^\circ$  Cone

STUREK

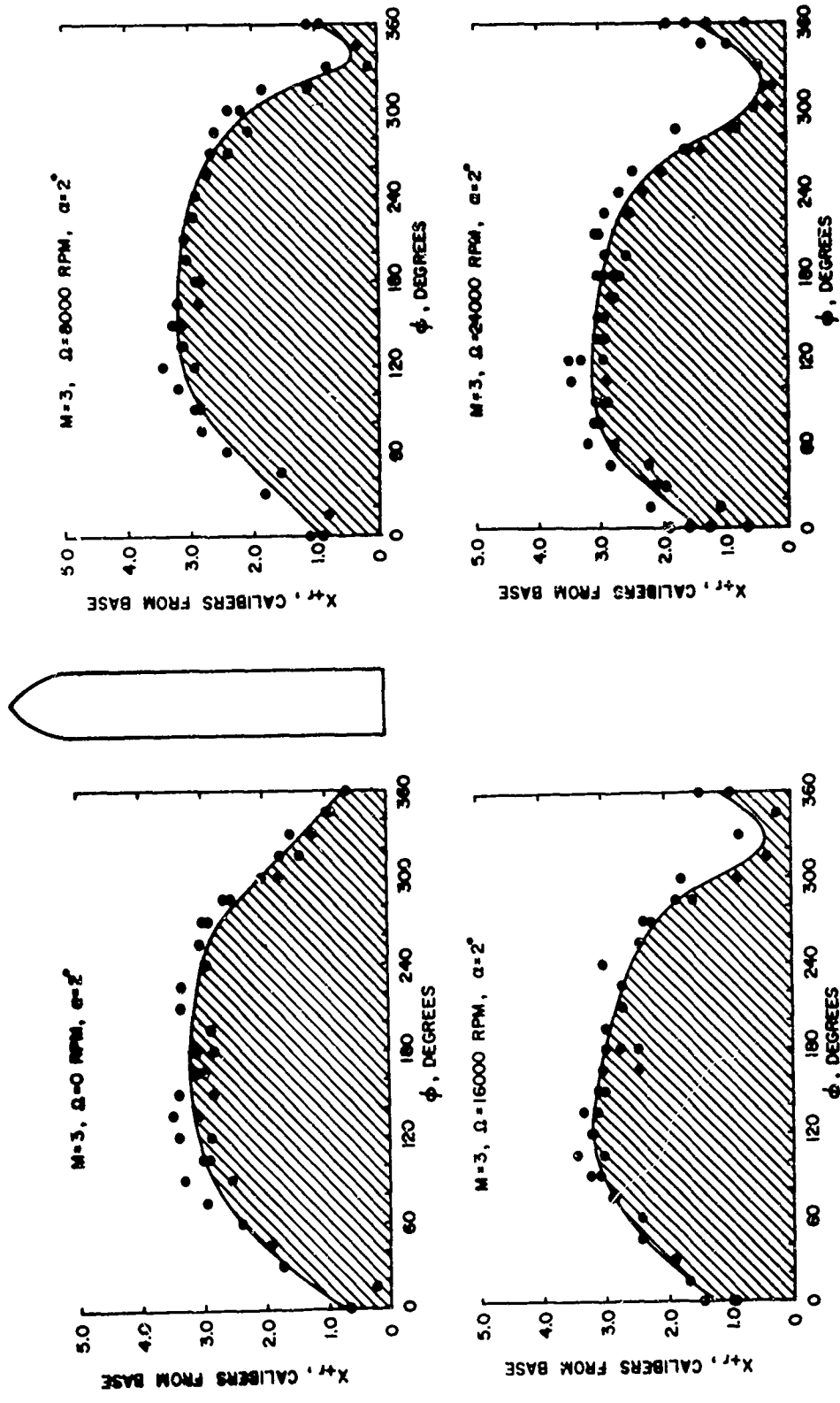


Figure 7. Profile of Boundary-Layer Transition About Circumference of Tangent-Ogive-Cylinder Model

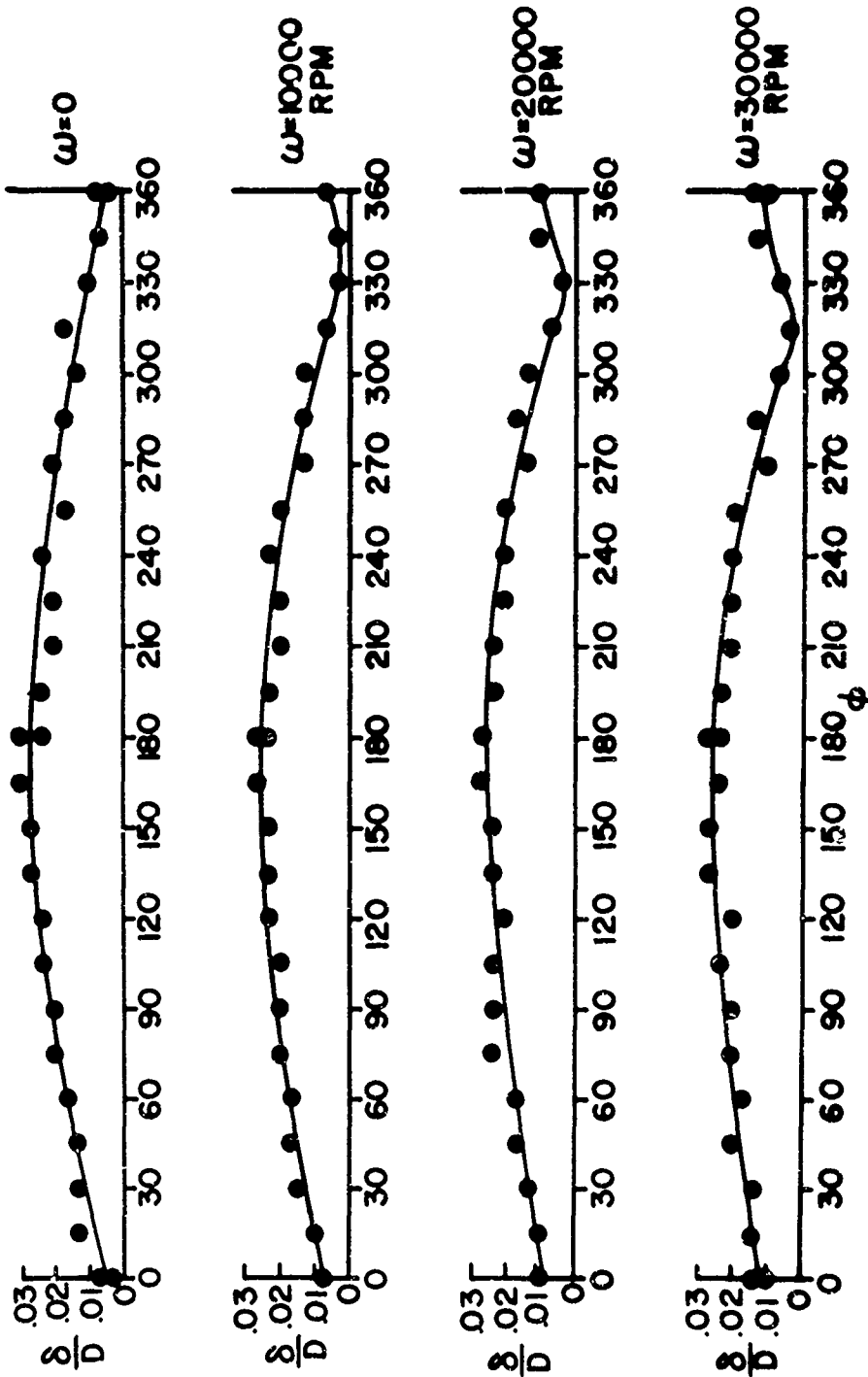


Figure 8. Distribution of Boundary-Layer Thickness About the Circumference of the Cone Model at the Base,  $M = 3$ ,  $\alpha = 2^\circ$ ,  $Re_\phi = 4.8 \times 10^6$

10° CONE MODEL

- PREDOMINATELY LAMINAR B.L.— $Re_x = 1.80 \times 10^6$
- - - PREDOMINANTLY TURBULENT B.L.— $Re_x = 6.1 \times 10^6$
- TRIPPED TURBULENT B.L.— $Re_x = 6.1 \times 10^6$

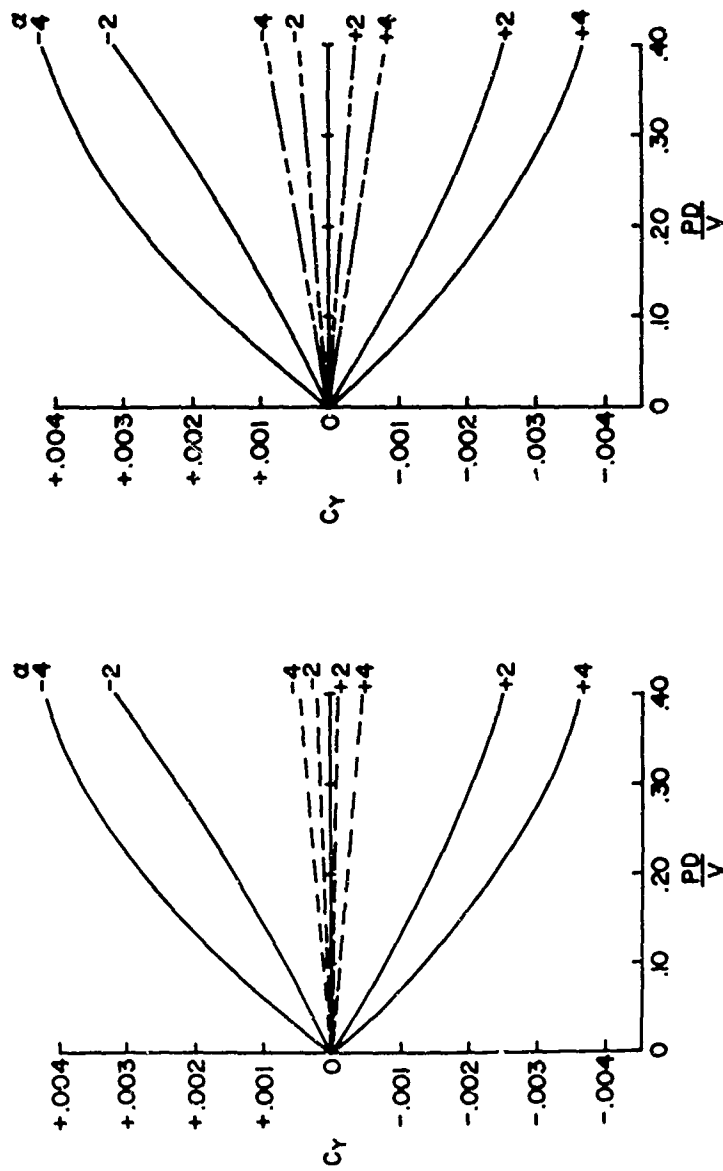


Figure 9. Magnus Coefficient Vs. Spin Rate for the Cone Model Comparing Measurements for Different Boundary-Layer Configurations,  $M = 2$

SIX CALIBER TANGENT-OGIVE-CYLINDER MODEL  
 ——— PREDOMINANTLY LAMINAR B.L.— $Re_0 = 0.59 \times 10^6$   
 - - - PREDOMINANTLY TURBULENT B.L.— $Re_0 = 1.06 \times 10^6$   
 - - - - TRIPPED TURBULENT B.L.— $Re_0 = 1.06 \times 10^6$

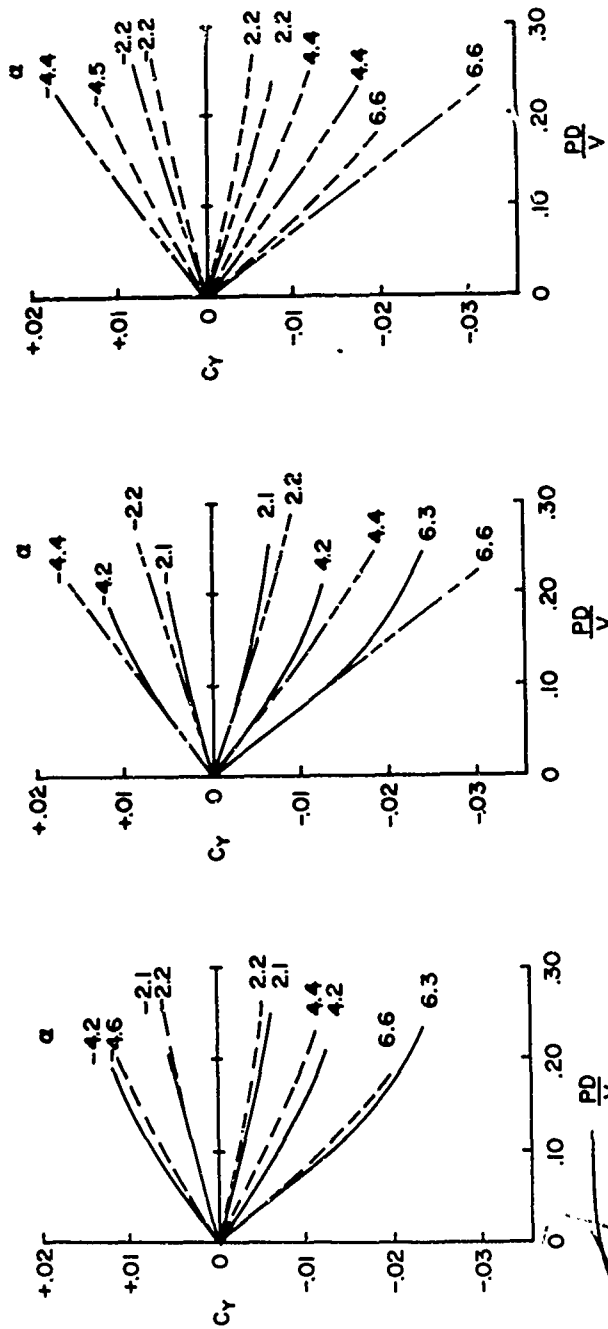


Figure 10. Magnus Coefficient Vs. Spin Rate for the Tangent-Ogive-Cylinder Model Comparing Measurements for Different Boundary-Layer Configurations,  $M = 3$